Eur. Phys. J. B **2**, 107–119 (1998)

THE EUROPEAN PHYSICAL JOURNAL B

Monte Carlo simulations of high-moment – low-moment transitions in Invar alloys

M.E. Gruner[a], R. Meyer, and P. Entel

Theoretische Tieftemperaturphysik, Gerhard-Mercator-Universität – Gesamthochschule – Duisburg, 47048 Duisburg, Germany

Received: 9 September 1996 / Revised: 23 May and 23 September 1997 / accepted: 3 September 1997

Abstract. We have reproduced magneto-volume effects typical for Invar alloys by examining a spin-analogous model which describes coupled spatial and magnetic degrees of freedom and, additionally, chemical disorder. Constant pressure Monte Carlo simulations of this model show an almost vanishing thermal expansion over a broad range of temperatures below T_{C}, a softening of the bulk modulus and the absence of a sharp peak in the specific heat at the magnetic phase transition as observed in $Fe_{65}Ni_{35}$ Invar.

PACS. 75.50.Bb Fe and its alloys – 75.80.+q Magnetomechanical and magnetoelectric effects, magnetostriction – 75.40.Cx Static properties (order parameter, static susceptibility, heat capacities, critical exponents, etc.)

1 Introduction

Since the discovery at the turn of the century that $Fe_{65}Ni_{35}$ exhibits an almost vanishing thermal expansion at room temperature [1], many experimental and theoretical investigations (for recent reviews on this topic see [2–4]) have taken place in order to explore anomalously low or high thermal expansion in various materials, generally called Invar or anti-Invar effect, respectively. Especially *ab initio* band structure calculations, which can determine the dependence of the internal energy on the mean magnetic moment and the lattice constant, play an important role in finding an explanation for this behavior (*e.g.* [4–6]). Recent calculations concerning $Fe_{65}Ni_{35}$ [6] using the KKR-CPA formalism revealed that the binding surface, which shows the energy as a function of the mean magnetic moment and the lattice constant, has two distinct, nearly degenerate minima: One at a lattice constant of 6.62 a.u. and a magnetic moment per atom of $1.6\,\mu_{\mathrm{B}}$ and another at a lattice constant of 6.48 a.u. and an almost vanishing magnetic moment. For the sake of simplicity we will call these minima high-moment state (HM) and low-moment state (LM), respectively. This result gives some late justification for the phenomenological two-γ-states model proposed by Weiss [7], which describes the properties of iron in a face-centered cubic environment by assuming two electronic states of the iron atom with different magnetic moments and different volumes.

Generally, those *ab initio* energy surfaces are calculated for zero temperature only, because extrapolating the results to finite temperatures faces severe methodological and technical problems. This hampers the comparison with experimental results, since most of the astonishing features of Invar alloys are observed at finite temperatures. So far, to the authors' knowledge, only continuous Ginzburg-Landau like spin models, which have been extended to finite temperatures by using a Gaussian fluctuation theory for magnetic and lattice degrees of freedom [8–12] have been used to fill this gap. Given the assumption that the HM-LM characteristic is the most important feature of the energy surface of Invar alloys, one may also investigate a Weiss type model, adapted to incorporate the results given by $T = 0$ *ab initio* calculations. For this purpose we used an approach previously taken by Takahashi [13,14], who proposed an Ising like spin model with coupled magnetic and spatial degrees of freedom for the description of low-moment – high-moment transitions occurring in some transition metal complexes. We modified this model to meet the situation in Invar alloys and employed the constant pressure Monte Carlo method, which allows us to calculate the temperature dependence of important properties as thermal expansion coefficient, adiabatic bulk modulus or specific heat and compare them with experimental data.

The use of a variation of the Weiss model and the neglect of the itinerant character of the 3d electrons in this paper needs further justification. To this we briefly discuss the magnetic binding surface of elemental fcc iron, since the origin of magnetovolume instabilities of the Invar-type in the Fe-Ni alloys and of the anti-Invar-type in the Fe-Mn alloys is related to the properties of γ-iron. Figure 1 shows the energy surface of γ-Fe with contour lines at 1 mRy/atom intervals in the moment *versus* volume (Wigner-Seitz radius) plane as obtained

[a] e-mail: me@thp.uni-duisburg.de

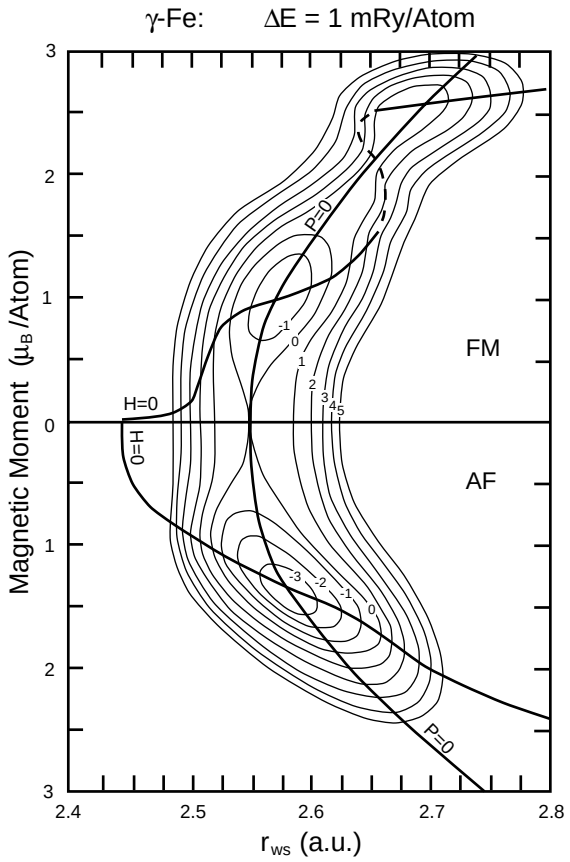

Fig. 1. Energy surface of γ-Fe for ferromagnetic (FM) and antiferromagnetic (AF) spin orientations estimated from *ab initio* calculations [15]. Contour lines are at $\Delta E = 1$ mRy intervals.

by an extrapolation of a zero-temperature full-potential calculation (semi-relativistic calculation using the full potential linearized augmented plane wave method, FLAPW, and the generalized gradient approximation, GGA, [15]). The surface exhibits three distinct local minima, a LM state (with $M \approx 1\,\mu_{\rm B}$ at $r_{\rm ws} \approx 2.6$ a.u.), a HM state (with $M \approx 2.5\,\mu_{\rm B}$ at $r_{\rm ws} \approx 2.7$ a.u.), and an antiferromagnetic LM state (with $M \approx 1.3\,\mu_{\rm B}$ at $r_{\rm ws} \approx 2.6$ a.u.), and in addition contains a nonmagnetic saddle point at $r_{\rm ws} \approx 2.56$ a.u.. The antiferromagnetic LM state is lowest in energy in accordance with experiment (for growth of γ-iron on a substrate with appropriate lattice constant) and only at very expanded volume a crossover to a ferromagnetic HM state occurs in agreement with the behavior of the inter-atomic exchange coupling constant [16]. This antiferromagnetic exchange interactions between the iron atoms survives in the Fe-Ni alloys and only the strong ferromagnetic exchange interaction between the Fe-Ni and Ni-Ni atoms stabilizes the ferromagnetic HM state in the Invar alloys. Disorder effects in Fe-Ni further stabilize the antiferromagnetic nature of the Fe moments as shown by recent supercell calculations [6]. Therefore, we will use these basic exchange interactions as an ingredient of our Hamiltonian and neglect its volume dependence, because the driving force for the LM $\rightleftharpoons$ HM transitions in the Invar-alloys is triggered by the depopulation of HM states with decreasing volume or increasing temperature. Our Monte Carlo simulations show that an additional renormalization is not necessary in order to explain major properties of Fe-Ni alloys. If at low temperatures parameters of our model Hamiltonian are fixed so that properties of the binding surfaces and curves of γ-Fe and γ-Fe-Ni alloys are in quantitative agreement with *ab initio* results at zero temperature, then it can be expected that most of the important aspects of the solid state have been taken into account and that Monte Carlo simulations of spin and lattice fluctuations will give reasonable results.

In this context one should mention that an alternative description based on a compressible Ising model has recently been proposed [17,18]. In the latter work also the importance of the antiferromagnetism of the *magnetovolume active* Fe-Fe *bonds* has been outlined. However, thermodynamic properties like thermal expansion, bulk modulus or specific heat have not been evaluated by the authors, so that a comparison with our results is not possible.

As in any itinerant magnetic system, the energetic splitting between the HM and LM state on the binding surface is connected with the gain in exchange energy with respect to kinetic and electrostatic energy changes. The volume dependence of such terms or of Ligand field-like terms certainly plays a role.

However, the treatment of these effects in the presence of magnetovolume instabilities with *ab initio* methods at finite temperatures is so far an unsolved problem [19]. Therefore, in previous work of finite temperature effects in Invar and anti-Invar alloys, effective Ginzburg-Landau Hamiltonians have been used [8–12], which do not restrict the system to two magnetic states. Shortcoming of this procedure is connected with an overestimation of fluctuation effects and the appearance of first-order phase transitions due to the Gaussian ansatz for the fluctuating fields.

In the present work the procedure is similar, we formulate a spin Hamiltonian with lattice degrees of freedom, whereby parameters are fixed by comparison to *ab initio* results. However, this finite temperature treatment is much better, since the Monte Carlo method allows to solve the Hamiltonian at any temperature without any further approximations. So partial aim of this work is connected with comparing our finite temperature results with previous results of a Gaussian fluctuation theory, a mode-mode coupling theory for spin and volume degrees of freedom, and with predictions for finite temperatures which can be made on the basis of first principles results for Invar alloys. A critical report of this will be given in the conclusions.

After giving a concise description of the model and the simulation method used, we will present in detail our results and relate them to previous theoretical and experimental investigations of Invar alloys. We will start with the discussion of the properties of a simple HM-LM model that is restricted to atoms of only one type. Afterwards we will deal with the properties of an extended model

which can handle chemically disordered binary alloys. Our simulations on this matter were designed to reproduce important properties of Fe-Ni alloys. Finally we will examine the behavior of our model alloy at finite pressure.

2 The model

The crucial point in the construction of a model for HM - LM transitions is the consideration of different spin states at each site i of the lattice. Takahashi [13,14] assumed two classical spins σ_i^1, $\sigma_i^2 = \pm 1$ at each site, coupled by an interaction constant j. Different sites interact with each other *via* the sum $S_i = (\sigma_i^1 + \sigma_i^2)/2$ of the local spins with an interaction constant J. If the two local spins σ_i on a site are antiparallel to each other (LM state), S_i vanishes and the site does not interact magnetically with its neighbors. Sites with parallel aligned σ's (HM state) show a normal interaction of the Ising type. In order to incorporate magnetovolume coupling, we introduce a pair interaction between the sites which depends on their distance r_{ik} and spin states. The total Hamiltonian which can be split into a magnetic part H_m and a vibrational part H_v is then

$$H = \underbrace{-j \sum_i \sigma_i^1 \sigma_i^2 - J \sum_{<i,k>} S_i S_k}_{H_\mathrm{m}} + \underbrace{\sum_{<i,k>} U(r_{ik}, S_i, S_k)}_{H_\mathrm{v}} \ . \quad (1)$$

The brackets indicate a summation over nearest neighbors. In contrast to [13,14], where harmonic potentials were used, we have adopted a Lennard-Jones type of interaction since this form exhibits thermal expansion:

$$U(r_{ik}, S_i, S_k) = \begin{cases} 4\epsilon_\mathrm{L} \left(\left(\frac{d_\mathrm{L}}{r_{ik}} \right)^{12} - \left(\frac{d_\mathrm{L}}{r_{ik}} \right)^{6} \right), \ S_i S_k = 0 \\ 4\epsilon_\mathrm{H} \left(\left(\frac{d_\mathrm{H}}{r_{ik}} \right)^{12} - \left(\frac{d_\mathrm{H}}{r_{ik}} \right)^{6} \right), \ S_i S_k \neq 0 \end{cases} , \quad (2)$$

where $\epsilon_{\mathrm{L,H}}$ denotes the energy at the equlibrium neighbor distance $r_{ik} = 2^{1/6} d_{\mathrm{L,H}}$ for LM and HM potentials, respectively.

Due to the relation $\sigma_i^1 \sigma_i^2 = 2 S_i^2 - 1$, the magnetic contributions H_m can be written as a spin-1 Ising Hamiltonian

$$\tilde{H}_m = -\tilde{j} \sum_i S_i^2 - J \sum_{<i,k>} S_i S_k \ . \quad (3)$$

Hamiltonian (3) is also known as Blume-Capel model [20,21] which was originally used for the description of magnetic first order phase transitions in UO_2. However, in our case one has to take care of the twofold degeneracy of the LM state $S_i = 0$. So one must make sure that each occurrence of $S_i = 0$ is counted twice in the computation of thermodynamical averages: For each spin configuration the Boltzmann factor in the sum over states has to be weighted by a factor 2^{-n} with $n = \sum_i S_i^2$ which can be accounted for by a temperature dependent anisotropy constant $\tilde{j}$ (*e.g.* [22])

$$\beta\tilde{j} = 2\beta j + \ln g \ . \quad (4)$$

Here, g describes the statistical weight of the LM state compared to the HM state, which determines the fraction of nonmagnetic sites in the limit of infinite temperature. In order to achieve accordance to Hamiltonian (1) one must use $g = 2$, but in principle any other level of degeneracy can be accounted for.

For the description of binary alloys, *e.g.* Fe-Ni, we have to choose the exchange constants J_{ik} dependent on the kinds of atoms involved. Further the difference in energy between the HM-state and the LM-state as given by j_i may vary, too. This leads to the Hamiltonian

$$H = -2 \sum_i j_i S_i^2 - \sum_{<i,k>} J_{ik} S_i S_k + \sum_{<i,k>} U_{ik}(r_{ik}, S_i, S_k) \ , \quad (5)$$

where $j_i \in \{j_\mathrm{Fe}, j_\mathrm{Ni}\}$ and $J_{ik} \in \{J_\mathrm{FeFe}, J_\mathrm{FeNi}, J_\mathrm{NiNi}\}$. For the sake of simplicity the U_{ik} do not depend on the type of the interacting atoms.

3 Simulation method and calculated quantities

Using the Hamiltonians (1,5) we have done Monte Carlo simulations on a fcc lattice with $N = 6^3 \times 4 = 864$ sites and $N = 12^3 \times 4 = 6912$ sites, respectively, using periodic boundary conditions. On a IBM workstation model 590 we reached a performance of up to 30 000 site updates per second. $80\,000 - 100\,000$ lattice sweeps were performed for each temperature, starting with the final configuration of the previous temperature. The first 30 000 sweeps were used to allow the system to reach equilibrium. To ensure this, each run was carried out twice, the first one calculated while heating up the system, the second one upon cooling down. After every tenth sweep, data were gathered for thermal averaging.

One site update consists of two Monte Carlo steps. First a new spin state is chosen using the usual Metropolis algorithm. In order to include the vibrational degrees of freedom, a new trial position is chosen afterwards from a cubic region around the actual position. Again this state is immediately accepted if it is more favorable with respect to its energy than the former one or with probability $\exp(-\beta \Delta H)$, otherwise. In order to improve convergence, the size of the cube is determined by the condition that about half of these propositions are to be accepted. Additionally, after each lattice sweep we introduced another Monte Carlo step which adjusts the volume of the whole system by varying a scaling parameter that is used as a factor for each neighbor distance. As in the former cases a new value is accepted if it fulfills the Metropolis condition mentioned above except that now the quantity

$$\Delta \mathcal{H} = \Delta H - N \, k_\mathrm{B} T \, \ln (V'/V) \quad (6)$$

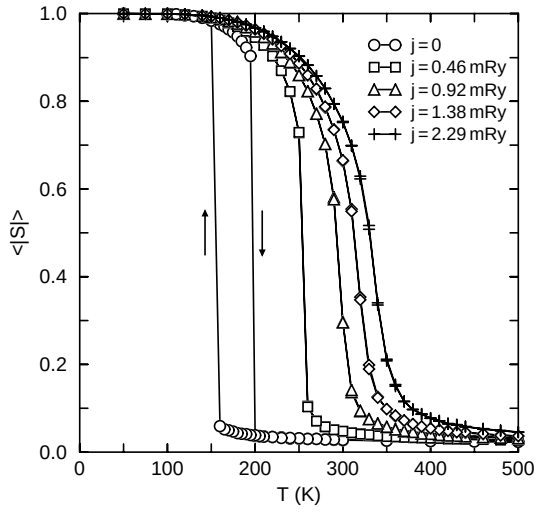

Fig. 2. Magnetization as a function of temperature in a monatomic system for different values of j ($J = 0.229\,\mathrm{mRy}$, $d_\mathrm{L} = 2.182\,\text{Å}$, $d_\mathrm{H} = 2.227\,\text{Å}$, and $\epsilon_\mathrm{L} = \epsilon_\mathrm{H} = 2.09\,\mathrm{mRy}$).

must be considered, where V' and V denote the new and the old volume of the simulation cell, respectively. The supplementary logarithmic term takes into account the difference in translational entropy caused by the change of the volume. For a more detailed description of constant pressure Monte Carlo methods see *e.g.* [23].

The restriction of making a volume adjustment only once per lattice sweep may lead for larger systems to a separation of the time scales of spin flip dynamics and lattice vibrations on the one side and volume adaption on the other side. However, this seems not to be too far-fetched for a realistic description of the elastic behavior of metals. Practically we observed that the equilibrium volume is reached after a few hundred lattice sweeps even if the simulation has started with a volume several percent apart from its equlibrium value. To ensure this, we compared the results for specific heat and thermal expansion coefficient, which can be calculated in two different ways: By numerically differentiating the mean values of energy and volume, and from the fluctuations of these two observables (see below). In our simulations, no significant differences were encountered. Therefore we suppose that relaxation time effects can be discarded.

In our calculations we considered the average magnetic moment, the absolute magnetization and the relative volume change

$$\langle S^2 \rangle = \left\langle \frac{1}{N} \sum_i S_i^2 \right\rangle \tag{7}$$

$$\langle |S| \rangle = \left\langle \frac{1}{N} \left| \sum_i S_i \right| \right\rangle \tag{8}$$

$$\omega = \frac{\langle V \rangle - V_0}{V_0}\,, \tag{9}$$

where V_0 designates the ground state volume of the simulation cell. Computing the magnetization of a binary alloy the different magnetic moments μ_i of the components must be regarded:

$$\langle |M| \rangle = \left\langle \frac{1}{N} \left| \sum_i \mu_i S_i \right| \right\rangle\,, \tag{10}$$

with $\mu_i \in \{\mu_\mathrm{Fe} = 2.8\,\mu_\mathrm{B}, \mu_\mathrm{Ni} = 0.6\,\mu_\mathrm{B}\}$ in the case of Fe-Ni alloys.

Furthermore we calculated the specific heat at constant pressure c_p, the linear thermal expansion coefficient α and the isothermal bulk modulus B_T [23]:

$$c_\mathrm{p} = \frac{1}{N\,k_\mathrm{B}\,T^2} \left(\left\langle (H + pV)^2 \right\rangle - \langle H + p\,V \rangle^2 \right) \tag{11}$$

$$\alpha = \frac{\langle V\,(H + p\,V) \rangle - \langle V \rangle \langle H + p\,V \rangle}{3\,k_\mathrm{B}\,T^2\,\langle V \rangle} \tag{12}$$

$$B_\mathrm{T} = k_\mathrm{B}\,T\,\frac{\langle V \rangle}{\langle V^2 \rangle - \langle V \rangle^2}. \tag{13}$$

The experimentally accessible adiabatic bulk modulus B_S can be obtained from (11-13) using the thermodynamical relations

$$\frac{B_\mathrm{T}}{B_\mathrm{S}} = \frac{c_\mathrm{v}}{c_\mathrm{p}} \qquad \text{and} \qquad c_\mathrm{p} - c_\mathrm{v} = 9\,\alpha^2\,T\,\frac{\langle V \rangle}{N}\,B_\mathrm{T}\,. \tag{14}$$

4 Simulations of monatomic systems

In a first step we examined the influence of the vibrational part H_v of the Hamiltonian (1). Therefore, we considered a homogenous system with atoms of one type only.

4.1 Fixing of the parameters

Since the ferromagnetic Invar effect has not been observed in pure metals but only in alloys, we did not adapt the parameters of our model to represent a particular material. The parameters have been chosen so that values for bulk modulus, thermal expansion coefficient and lattice constant typical for iron alloys as well as reasonable magnetic transition temperatures for disordered Fe-Pt alloys were obtained: $J = 0.23\,\mathrm{mRy}$, $d_\mathrm{L} = 2.182\,\text{Å}$, $d_\mathrm{H} = 2.227\,\text{Å}$, and $\epsilon_\mathrm{L} = \epsilon_\mathrm{H} = 2.09\,\mathrm{mRy}$. We set $\epsilon_\mathrm{L} = \epsilon_\mathrm{H}$ so that the difference in energy between pure HM and LM states were determined by the magnetic parameters j and J, only. The parameter j has been varied from $j = 0$ to $j = 2.29\,\mathrm{mRy}$. This choice of parameters induces a ferromagnetic HM ground state as is observed in real Invar materials.

4.2 Results

The magnetization per atom, Figure 2, shows continuous transitions as well as first order transitions from the ferromagnetic ground state to a paramagnetic high temperature state depending on the choice of j: Favoring the HM

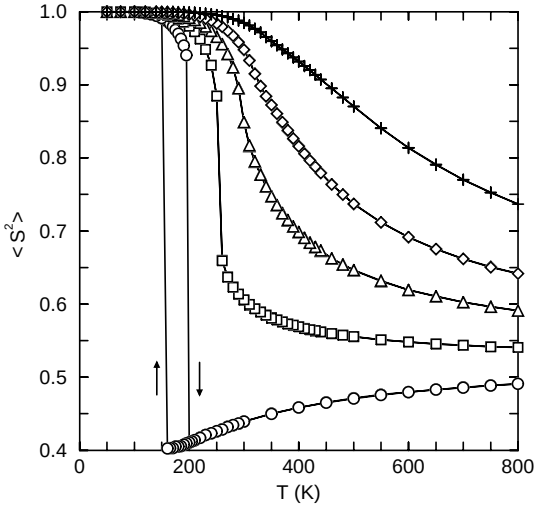

Fig. 3. $\langle S^2 \rangle$ as a function of temperature in a monatomic system. Same symbols and parameters as in Figure 2.

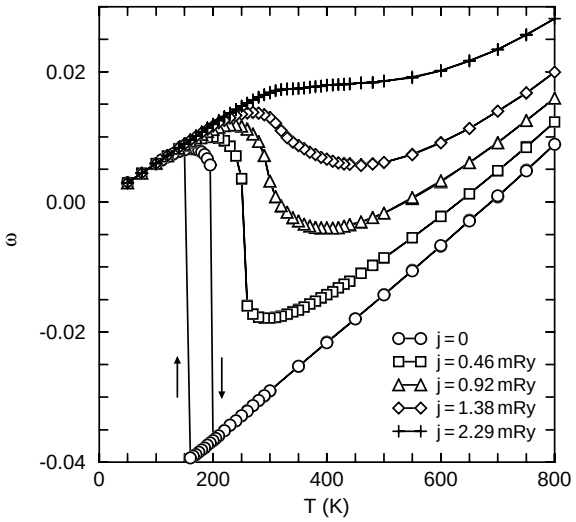

Fig. 4. Relative volume change as a function of temperature in a monatomic system. Same parameters as in Figure 2.

state by employing a large positive j leads to a continuous transition; in the limiting case $j \to \infty$ the LM state is not accessible and the system behaves like a spin-$\frac{1}{2}$ Ising model without any magnetovolume coupling. Lowering j causes a reduction of the transition temperature and a change of the critical behavior: The transition becomes first order and exhibits a considerable hysteresis. Respectively, the concentration of HM-Atoms $\langle S^2 \rangle$ shows an increasing dilution of magnetic sites at a given temperature with decreasing j (see Fig. 3). Also, at low j, an abrupt jump from a ferromagnetic HM state into a paramagnetic regime dominated by LM sites can be observed. Further lowering of j leads to a nonmagnetic ground state.

As expected, thermal agitation of LM sites results in a corresponding contraction of the simulation cell, as can be seen from Figure 4. Again, the change of the simulation volume at small j is discontinuous. At $j = 2.29$ mRy we find a more or less vanishing thermal expansion which would be typical for the Invar alloy $Fe_{65}Ni_{35}$ [2]. However, the minimal thermal expansion coefficient α is reached for a temperature considerably higher than T_C (see Fig. 5) which is in contradiction to experimental data. Lowering j leads to a coincidence of magnetic transition and minimal thermal expansion. At $j = 1.38$ mRy, where the energy associated with magnetic ordering and the difference in energy between HM and LM states are of about the same size, we find a sharp dip in α, which resembles with a minimal value of $\alpha_{\min} \approx -5 \times 10^{-5}$ K^{-1} the experimental findings in disordered $Fe_{72}Pt_{28}$ ($\alpha_{\min} = -4.7 \times 10^{-5}$ K^{-1}, [24]). Please note that we cannot reproduce Grüneisen behavior, since we are dealing with a classical description of the elastic degrees of freedom. Hence we will find a positive α even at $T = 0$.

Also, the adiabatic bulk modulus (Fig. 6) exhibits the expected weakening of the material which is in qualitative agreement with the behavior of real $Fe_{72}Pt_{28}$. The experimental data in Figure 6 are gained from ultrasonic measurements of the elastic constants C_L, C' and C_{44} [25] *via* the relation

$$B_S = C_L - \frac{1}{3}C' - C_{44} \,. \tag{15}$$

4.3 Discussion

The occurrence of a first order transition for $j = 0$ is caused by the vibrational part H_v of the Hamiltonian (1), since investigations concerning the magnetic contributions H_m only (*e.g.* [22,26]) reveal a second order transition with Ising critical behavior. Investigations of the ferromagnetic fcc Blume-Capel model (3) show that first order transitions occur for $\tilde{j}/(12J) < -0.47$ [27,28]. In our simulations, however, only nonnegative values of j have been used. It has to be pointed out, that our model is not a compressible Ising model in the classical sense [29], since in our model the magnetovolume coupling is achieved by introducing a third, nonmagnetic spin state with different elastic properties. Therefore, our results are not in contradiction with the extensive investigation of the compressible Ising model by Bergman and Halperin [30] who generally found second order phase transitions. The change of the phase transition from second order to first order due to the inclusion of a particular kind of volume dependent interactions is a well-known effect and occurs in many microscopic models (see *e.g.* the discussion of the periodic Anderson model coupled to static lattice distortions [31,32], or the discussion of the magnetic volume collapse in itinerant systems [10]). Transformations of the phonon coordinates lead to a strongly interacting electron or spin system with volume instabilities of first or

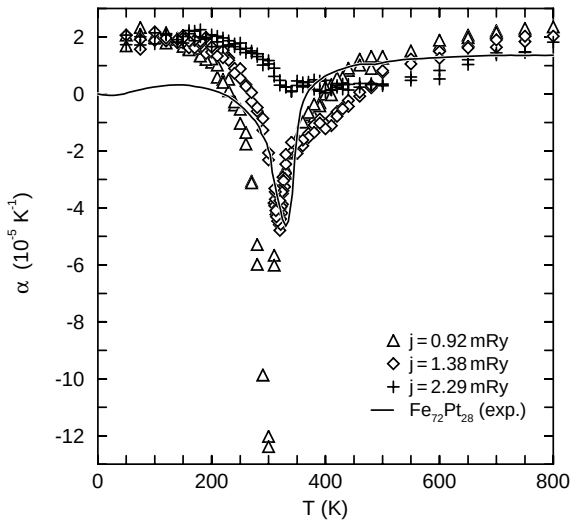

Fig. 5. Thermal expansion coefficient α as a function of temperature in a monatomic system. Same parameters as in Figure 2. The solid line denotes the experimental data for α for disordered $Fe_{72}Pt_{28}$ (taken from [24]).

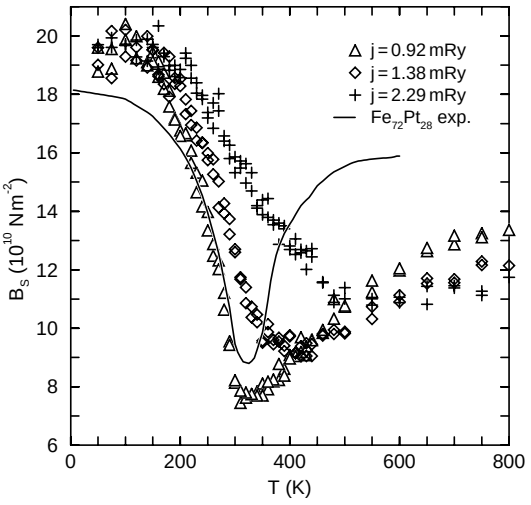

Fig. 6. Adiabatic bulk modulus B_S as a function of temperature in a monatomic system. Same parameters as in Figure 2. Experimental values for B_S are depicted by a solid line (after [25]).

second order depending on the parameters. Here it can be understood by a simplified discussion of the free energy. Since the ground state is ferromagnetic and without elastic distortions, we will have an absolute minimum for the pure HM state at low temperatures. For a suitable choice of j, an undistorted, LM dominated regime at a lower volume, determined by the LM Lennard-Jones pair potentials, will establish a second minimum. This LM regime may contain some HM sites without showing up elastic distortions, because HM pair potentials only apply if both sites are HM. These minima are separated by a large energy barrier, since the intermixing of HM and LM pair potentials, which is inevitable for heterogeneous regimes, is suppressed by H_v. With increasing temperature, entropy will drag the LM minimum below the HM minimum without compensating the energy barrier in between, thus leading to a first order HM-LM transition. At higher temperatures, the influence of H_v diminishes since the lattice becomes distorted anyway, due to lattice vibrations. Or, to put it the other way round, the switching of the magnetic moment does not contribute significantly to the lattice strain anymore. On the other hand, if a sufficiently high j suppresses the LM state, thermal excitation of single LM sites is the dominating process, leading to a smooth decline of the mean magnetic moment towards its high temperature limit. The HM-LM transition has disappeared. In this case, lattice vibrations do not have any serious effect on the breakdown of the magnetic order. The phase transition will presumably exhibit Ising universality, as found in annealed diluted Ising systems [22,26]. Indeed, for $j = 1.38$ mRy and $j = 0.92$ mRy scaling plots of magnetization, susceptibility and specific heat for linear system sizes $L = 4 \ldots 12$ seem to be consistent with the assumption of Ising criticality. We achieved the best data collapses with the following values (α, β, γ denote the exponents of specific heat, magnetization and susceptibility, respectively. The critical temperature T_C and the exponent ν of the correlation length were determined from the Binder cumulant [33]): For $j = 1.38$ mRy: $T_C = 321.7$ K, $1/\nu = 1.6 \pm 0.1$, $\alpha/\nu = 0.18 \pm 0.03$, $\beta/\nu = 0.51 \pm 0.03$, $\gamma/\nu = 1.98 \pm 0.04$. For $j = 0.92$ mRy: $T_C = 299.1$ K, $1/\nu = 1.6 \pm 0.1$, $\alpha/\nu = 0.19 \pm 0.03$, $\beta/\nu = 0.50 \pm 0.03$, $\gamma/\nu = 2.00 \pm 0.04$. For $j = 0.46$ mRy we were not able to produce a data collapse with Ising-like exponents. The systems are much too small to provide a reliable estimation, but this gives us a hint, that the first-order transition may vanish between $j = 0.46$ mRy and $j = 0.92$ mRy.

A striking feature of the first order transitions is the large thermal hysteresis which suggests that the system faces problems in reaching the thermodynamic equilibrium in time. This effect can be traced back to the large energy barrier between the ferromagnetic HM state at high volume and the paramagnetic mixed LM state at low volume. Such a barrier is hard to overcome for the global MC step used for the volume adaption, especially when fluctuations diminish with decreasing temperature. Since this energy barrier will vary with the number of atoms to be moved, the width of the hysteresis loop varies with system size and the number of lattice sweeps. In the extreme, the system does not find back to its ground state upon cooling down. First order transitions with thermal hysteresis, comparable to the ones described in this work can be found in manganese compounds like YMn_2 [34,35]: This compound shows an discontinuous shrinking of the lattice parameter around $T = 100$ K, which is connected

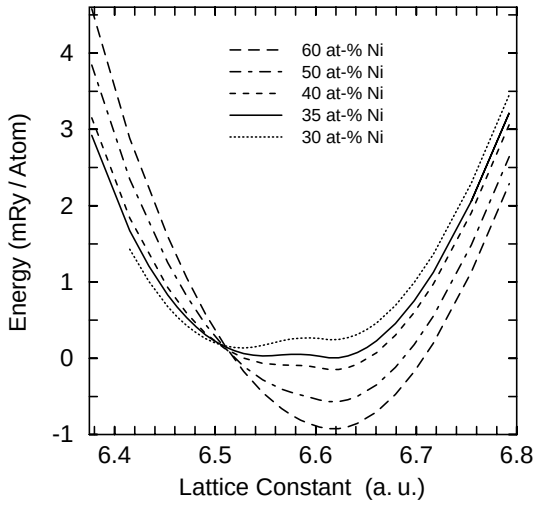

Fig. 7. Energy per lattice site at $T = 4\,\mathrm{K}$ as a function of the lattice constant for different compositions of $Fe_{1-x}Ni_x$.

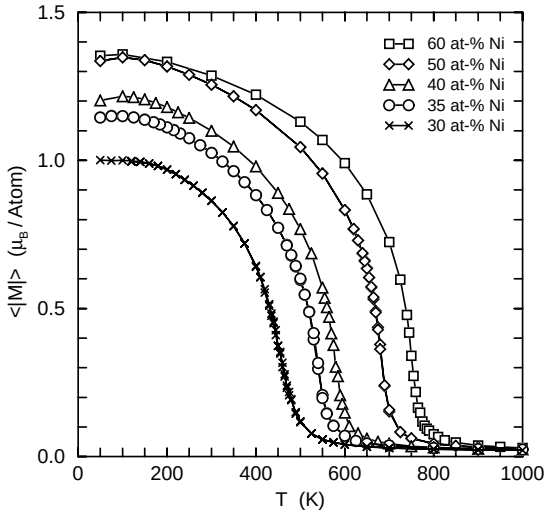

Fig. 8. Magnetization as a function of the temperature for different compositions of $Fe_{1-x}Ni_x$.

with an abrupt loss of the magnetic moment. However, one has to keep in mind that YMn_2 occurs in the cubic Laves phase with an antiferromagnetic order of the manganese atoms, which is not the situation in our simulations.

The continuous transitions which we investigated are in some aspects (thermal expansion coefficient, adiabatic bulk modulus) in qualitative accordance with experimental data for $Fe_{72}Pt_{28}$. This supposes that a simple statistical model as the one described here might be a useful tool for studying HM-LM transitions in Invar materials. On the other hand magnetovolume effects smeared out as in $Fe_{65}Ni_{35}$ and a flattening of the specific heat c_p are not reproduced. Instead we expect Ising universality which is connected with a sharp divergence of the specific heat at T_C. This shows that some refinement of the model is necessary in order to obtain an adequate description of magnetovolume effects in Invar alloys.

5 Simulations of alloys with chemical disorder

One way to improve the model is the introduction of different types of atoms with different magnetic behavior placed in quenched random disorder on the lattice. In this case the energy associated with the ferromagnetic alignment of the spins depends on the types of surrounding atoms. Since this energy has to be overcome in order to flip a spin into the LM state, chemical disorder will smear out magnetovolume effects over a large range of temperatures below T_C.

5.1 Details of the calculations

As a reference alloy we chose Fe-Ni, since the binding surfaces for various compositions are known from KKR-CPA calculations [6]. These show for the Invar concentration $Fe_{65}Ni_{35}$ two distinct, nearly degenerate minima of the energy in the volume-magnetization plane. Besides that, previous papers show [36,37] that the Ni-rich part of the magnetic phase diagram can be approximated by an Ising model with three different exchange constants J_FeFe, J_FeNi and J_NiNi. These calculations, however, did not take into account the existence of the LM state of the iron atoms and neglected vibrational degrees of freedom. In both papers antiferromagnetic couplings between iron atoms ($J_\mathrm{FeFe} < 0$) were chosen in order to achieve a better fit to experimental data, while the other exchange constants remained positive. This causes some iron moments to be aligned antiparallel in the mainly ferromagnetic ground state which leads to a deviation of the spontaneous magnetization from the Slater-Pauling curve at large iron contents. A further motivation for the selection of antiferromagnetic Fe-Fe exchange couplings is given by *ab initio* calculations of γ-iron by Sabiryanov *et al.* [16]. These show that the exchange coupling of an effective Heisenberg model depends sensitively on the distance between nearest neighbors: It is large and positive for distances above $d_\mathrm{NN} > 2.595\,\text{Å}$ and vanishes below $d_\mathrm{NN} < 2.52\,\text{Å}$. In between the exchange constant takes on large negative values. For the same reason, the choice of $J_\mathrm{FeFe} < 0$ is not in contradiction to our previous calculations, which describes properties of $Fe_{72}Pt_{28}$ by taking only ferromagnetic interactions into account: Fe-Pt alloys are known to have a larger lattice constant than Fe-Ni alloys.

In our simulations we took $J_\mathrm{NiNi} = 0.40$ mRy, which reproduces T_C of pure nickel, $J_\mathrm{FeNi} = 0.96$ mRy and $J_\mathrm{FeFe} = -0.72$ mRy. J_FeFe is chosen about twice as large in its absolute value compared to [36,37], so that a reasonable transition temperature for $Fe_{65}Ni_{35}$ is reproduced. This leads, however, to deviations in T_C on

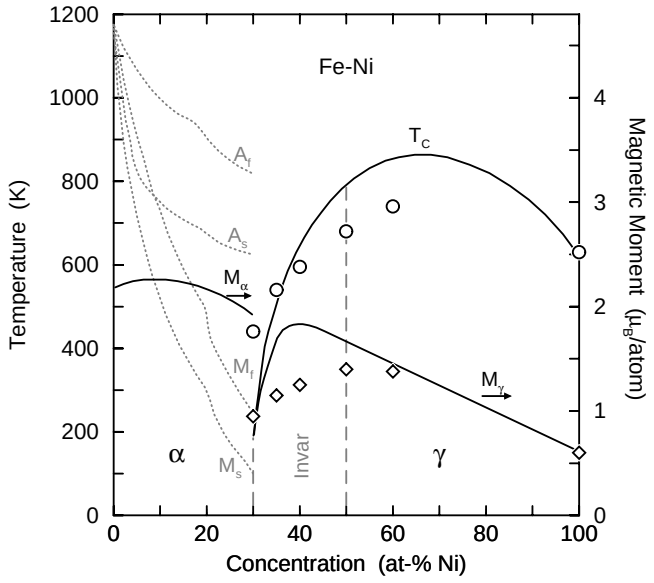

Fig. 9. Calculated Curie temperature and spontaneous magnetization (denoted by circles and diamonds, respectively) for various compositions of $Fe_{1-x}Ni_x$ in comparison with experimental data (taken from [39]). M_s, M_f, A_s and, A_f denote the start and final temperatures of the martensitic and austenitic phase transition.

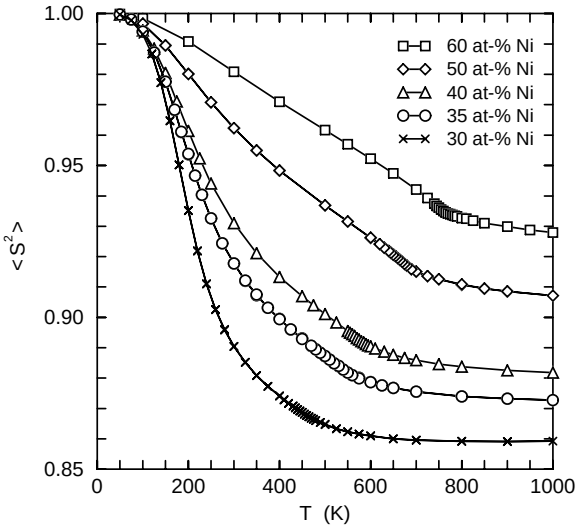

Fig. 10. Concentration of HM atoms as a function of the temperature for different compositions of $Fe_{1-x}Ni_x$.

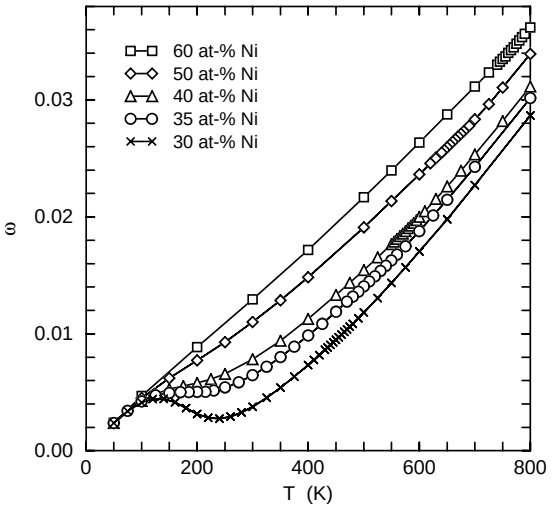

Fig. 11. Relative volume change as a function of the temperature for different compositions of $Fe_{1-x}Ni_x$.

the Ni-rich part of the phase diagram. Since pure nickel does not exhibit a negative anomaly in the thermal expansion coefficient we disallowed the LM state for all nickel atoms by choosing $j_{\mathrm{Ni}} \gg k_{\mathrm{B}}T$. By disadvantaging the magnetic state of the iron atoms ($j_{\mathrm{Fe}} = -1.10$ mRy) we achieved that two nearly degenerate minima of the internal energy as a function of the atomic volume show up as postulated by KKR-CPA calculations [6]. From the same source we took the HM and LM equilibrium neighbor distances $d_{\mathrm{H}} = 2.209\,\mathrm{\AA}$ and $d_{\mathrm{L}} = 2.165\,\mathrm{\AA}$. Finally, with $\epsilon_{\mathrm{H}} = \epsilon_{\mathrm{L}} = 25.47\,\mathrm{mRy}$, we obtained a reasonable bulk modulus for Fe-Ni alloys. The statistical weight of the nonmagnetic state has been set to $g = 0.5$ in order to restrict the fraction of nonmagnetic sites at infinite temperature to 20%. This is the same value as in a spin-2 model and in accordance with considerations of Holden *et al.* [38], which predict that in $Fe_{65}Ni_{35}$ above T_{C} a fraction of 15% to 35% of the iron atoms is in the LM state.

Our calculations were performed on a $12^3 \times 4 = 6912$ site fcc lattice, which is still too small to rule out effects of the specific lattice configurations used. So runs with larger system sizes and averaging over ensembles of lattice configurations would be desirable but were not possible up to now due to our time consuming simulation method. The observed magnetoelastic effects, however, can be expected to be reliable, because they occur, as we will point out later, far below the magnetic phase transition, whereby at T_{C} considerable size and configuration dependent effects have to be assumed. Indeed, calculations with much smaller systems (500 Atoms) revealed some restricted quantitative deviations in the absolute values of our observables, but no qualitatively different behavior at all throughout the whole temperature and concentration range covered. Additionally, we repeated our calculations for 35 at-% Ni in the vicinity of the phase transition with 6912 Atoms and same parameters but a different lattice configuration. We found that the results for $\langle |M| \rangle$, $\langle |S^2| \rangle$, ω and the internal energy are nearly indistinguishable,

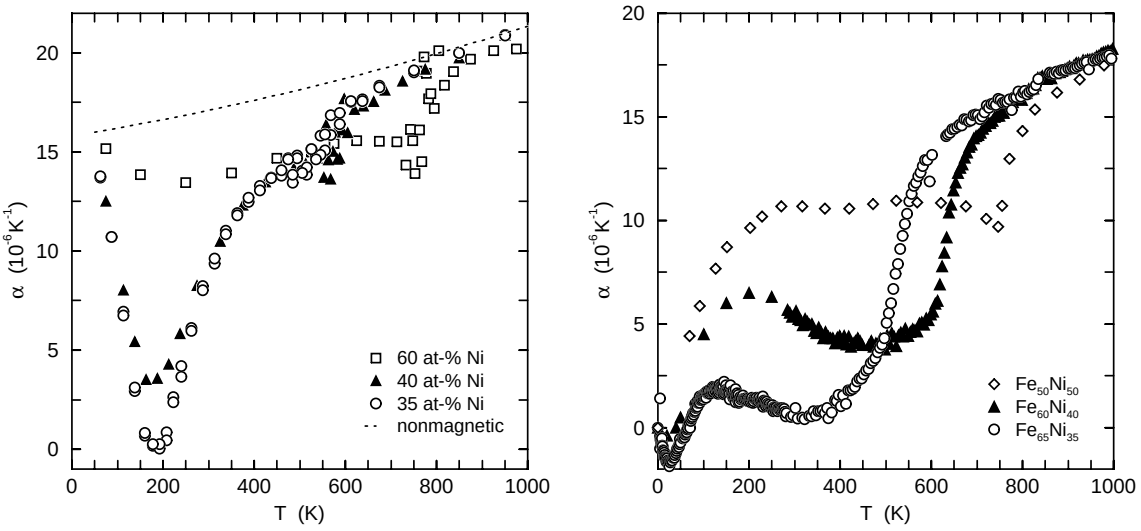

Fig. 12. Calculated (left) and experimental (right) thermal expansion coefficient as a function of the temperature for different compositions of $Fe_{1-x}Ni_x$ and a nonmagnetic reference system. Experimental data were taken from [42].

the deviations lie clearly within the size of the symbols. This shows that the main properties of the model are well described by the specific lattice configuration used. We examined compositions containing 30 . . . 60 at-% Ni. At lower nickel concentrations, Fe-Ni alloys undergo a martensitic transformation to a bcc phase that does not show the magnetovolume effects we are interested in. Additionally we computed specific heat and elastic properties of a nonmagnetic reference sample which is characterized by nearest neighbor Lennard-Jones potentials (2) and the constants d_{H}, ϵ_{H}.

5.2 Results

We approximated the ground state energy per atom as a function of the volume by exponentially cooling down the sample to $T = 4$ K (Fig. 7). As mentioned above, we find for the Invar concentration (35 at-% Ni) two nearly degenerate minima establishing the negative anharmonicity which is responsible for the Invar effect. With increasing nickel content, the LM minimum becomes energetically less favorable and seems to vanish at about 60 at-% Ni. *Vice versa*, for larger iron concentrations the HM minimum becomes disadvantageous. These observations are in qualitative accordance with the *ab initio* calculations [6], although the energy differences between the minima are smaller in our calculations.

Figure 8 shows the magnetization of the alloy as a function of the temperature. As expected, T_{C} increases with increasing nickel content on the iron rich side as well as the reduction of the spontaneous magnetization vanishes due to the antiparallel alignment of the iron atoms. However, the calculated Curie temperatures are too small on the nickel rich side and the deviations from the Slater Pauling curve are too large in comparison with experimental data (Fig. 9). As mentioned above, these results are due to an overestimated exchange constant J_{FeFe} for the Ni-rich side. A better fit to the phase diagram could be achieved by choosing J_{FeFe} for each concentration separately. But this is, as we will see, not necessary for a qualitatively correct reproduction of the anomalies of Fe-Ni Invar.

Increasing the iron content results in a steeper decrease of the concentration of HM atoms (Fig. 10), resembling the effect of reducing the anisotropy j in our calculations for the pure system (Fig. 3). In contrast to Figure 3 the largest change in $\langle S^2 \rangle$ takes place at temperatures below the magnetic phase transition. At the magnetic phase transition the fraction of HM atoms has almost reached its high temperature limit which implies that at the Invar concentrations around T_{C} almost no magnetovolume effects should be observed. This expectation is confirmed by Figure 11 and Figure 12 which show plots of the relative volume change ω and thermal expansion coefficient α as a function of temperature. Accordingly the main impact on ω is observed at temperatures far below T_{C}. For 35 at-% Ni, thermal expansion nearly vanishes at about 200 K ($T_{\mathrm{C}} \approx 540$ K). In real $Fe_{65}Ni_{35}$ ($T_{\mathrm{C}} = 503$ K) the corresponding minimum in the thermal expansion is observed at room temperature. Both, calculated and experimental curves seem to be smooth around T_{C}. On the nickel rich side, our calculations indicate a slight dip in α at the magnetic phase transition which corresponds to a similar anomaly in the experimental data. The change of the shape of the curves with increasing nickel content can be easily explained in the framework of our model: The diminishing number of antiferromagnetic Fe-Fe exchange couplings discourages excitations of spins into the LM state, since the ferromagnetic order is stabilized. So HM-LM flips will more likely occur around T_{C} where this order is about to vanish.

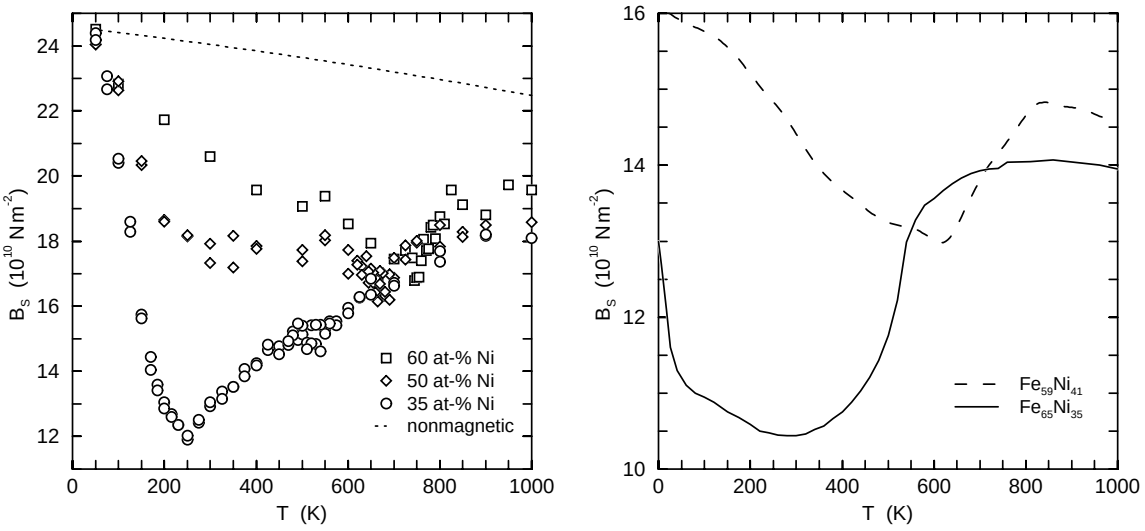

Fig. 13. Left: Calculated bulk modulus as a function of the temperature for different compositions of $Fe_{1-x}Ni_x$ and a nonmagnetic reference system. **Right:** Experimental Bulk moduli of $Fe_{65}Ni_{35}$ [40] and $Fe_{59}Ni_{41}$. The latter was determined from ultrasonic measurements of elastic constants [41,2] *via* Eq. (15).

Again the low temperature behavior is not reproduced correctly due to the employment of a classical model. A further drawback is that our simulations do not yield anti-Invar behavior for 30 at-% Ni. In contrast to experimental observations we find even a contraction of the material.

Increasing the iron content also leads to an enhanced weakening of the material around $T \approx 200\,\mathrm{K}$, as can be seen from the adiabatic bulk modulus B_S (Fig. 13). Since B_S is derived from the fluctuations of the mean volume per atom (13-14) which is closely related to the concentration of HM atoms, we find the maximum effect at temperatures where $\langle S^2 \rangle$ has its maximum slope. Although the magnitude of the anomaly is exaggerated by our calculations, calculated and measured bulk moduli for $Fe_{65}Ni_{35}$ show a rather similar behavior: A steep decrease at low temperatures, a broad minimum coinciding with the anomaly in α and a smooth increase around T_C. On the other hand, the zigzag like anomaly in B_S around T_C in the experimental curve for $Fe_{59}Ni_{41}$ resembles our calculated curves for higher nickel content. Figure 13 also suggests that between 40 and 50 at-% Ni B_S may be nearly constant around room temperature. This is a hint that our model alloy may also show Elinvar behavior which is experimentally observed at about 45 at-% Ni.

Our plots of the specific heat c_p (Fig. 14) exhibit, that with increasing iron content the sharply peaked anomaly at T_C evolves to a broadened and flattened cusp which agrees with experimental results for the specific heat of Fe-Ni alloys [43]. Indeed a change in the critical behavior with increasing iron concentration must be expected, since the phase transition in a fcc Ising antiferromagnet is of first order (*e.g.* [44,45]). Above T_C, we find a large enhancement of c_p in comparison with the nonmagnetic reference curve, which is also experimentally observed. When comparing the calculated values of c_p with experimental data, one has to bear in mind that our model Hamiltonian (5) is missing a kinetic part which has a contribution of about $3/2\,R = 12.5\,\mathrm{J\,mol^{-1}\,K^{-1}}$. Around $T = 200\,K$ the systems with larger iron content show an additional maximum. This can be interpreted as a Schottky anomaly due to the enhanced number of thermal excitations to the LM state. The experimental curves for $Fe_{50}Ni_{50}$ and $Fe_{60}Ni_{40}$ also show a second anomaly below T_C. In contrast to our calculations, this anomaly shows up at relatively high nickel concentrations and disappears at lower nickel concentrations, where HM-LM excitations are easier. Recent measurements of c_p [42] do not show this behavior and seem therefore to be in better agreement with our calculations.

Since the concentration of LM atoms is only 12% around T_C, the disappearance of the specific heat peak is rather caused by the increased number of antiferromagnetic exchange couplings. The smearing out of c_p does not contradict the Harris criterion [46], which states that disorder is relevant in three dimensions if the critical exponent of the specific heat α is positive, irrelevant if negative, because in case of disorder we have

$$u\,|t|^{-\Phi_u} \propto |t|^{-\alpha/2} \tag{16}$$

$$\text{with} \quad t = \frac{|T - T_\mathrm{C}|}{T_\mathrm{C}}, \quad \Phi_u \approx 1, \tag{17}$$

$$\text{and} \quad u = \frac{1}{\xi^3 \langle J \rangle} \sqrt{\int_{\xi^3} \mathrm{d}^3 r \, \left\langle \left(J(\mathbf{r}) - \langle J \rangle \right)^2 \right\rangle} \propto \xi^{-3/2}, \tag{18}$$

where Φ_u is the crossover exponent, $J(\mathbf{r})$ is the interaction at $\mathbf{r}$ and ξ the correlation length; the brackets stand for

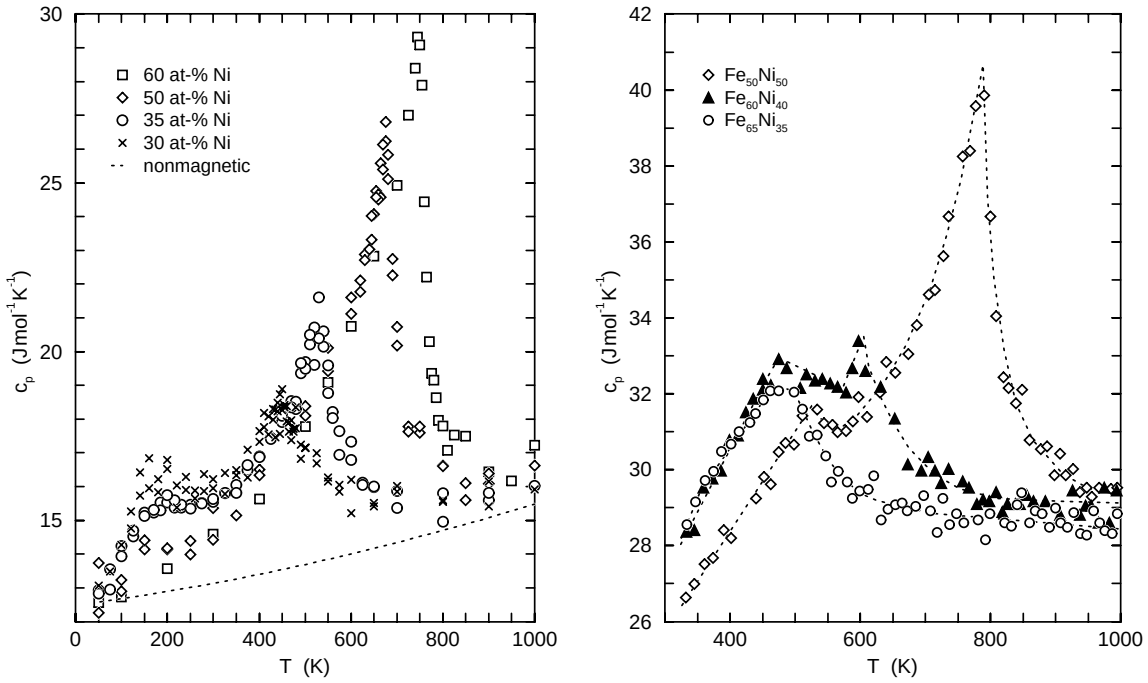

Fig. 14. Left: Calculated specific heat c_p as a function of the temperature for different compositions of $\mathrm{Fe}_{1-x}\mathrm{Ni}_x$ and a nonmagnetic reference system. **Right:** Specific heat as given by experiment [43]. The dashed lines are guide to the eye.

the averaging with respect to the *impurity distribution function*. In addition hyperscaling, $3\nu = 2 - \alpha$, has been used. However, this only holds if all $J(\mathbf{r})$ have the same sign. Our model corresponds to strongly disordered systems in the sense, that similar to a spin glass we have ferro- and antiferromagnetic interactions. In addition the coupling to the volume lead to a distribution of HM and LM domains which sizes are temperature dependent. For the concentrations investigated, the authors do not exclude, that, due to the dominance of remaining ferromagnetic interactions, there is still a narrow region of temperature, in which the infinite system exhibits a sharp divergence of c_p. However, if this critical region is small enough, simulations on finite systems and presumably experiments as well will show a broad smearing out of the specific heat peak (as is the case for all Invar alloys).

5.3 Simulations at finite pressure

It is known from Mössbauer measurements of the pressure dependence of the hyperfine field, that magnetism in Fe-Ni alloys around the Invar concentration breaks down if the external pressure is high enough [47,48]. The authors found, that in $\mathrm{Fe}_{68.5}\mathrm{Ni}_{31.5}$ with increasing pressure Curie temperature and average hyperfine field diminish. At a critical pressure $p_\mathrm{c} = 5.8$ GPa they observe a discontinuous drop in both quantities to a value near zero. Since our simulation method allows calculations for any given pressure, we examined the magnetization of $\mathrm{Fe}_{65}\mathrm{Ni}_{35}$ as a function of the external pressure for two temperatures $T = 50$ K and $T = 300$ K. In Figure 15 the calculated magnetizations are shown in comparison with experimental values of the average hyperfine field at $T = 4.2$ K in $\mathrm{Fe}_{65}\mathrm{Ni}_{35}$ and $\mathrm{Fe}_{68.5}\mathrm{Ni}_{31.5}$ [47]. In any case both, calculated magnetization and hyperfine field, decrease with increasing pressure. At low temperatures the pressure dependence of the calculated magnetization is in fairly good agreement with the Mössbauer data for $\mathrm{Fe}_{65}\mathrm{Ni}_{35}$, but experimental values for pressures above 10 GPa would be desirable to confirm this correspondence. On the other hand a sharp drop of the magnetic moment like the one observed in $\mathrm{Fe}_{68.5}\mathrm{Ni}_{31.5}$ is not reproduced by our calculations. At $T = 300$ K we find a phase transition at a critical pressure $p_\mathrm{c} \approx 18$ GPa. This is about three times higher than we would expect for the real alloy [47]. At $T = 50$ K no such peak occurs. The magnetization approaches a steady value of $0.21\,\mu_\mathrm{B}$ which corresponds to all iron atoms being in the LM state and all nickel atoms aligned in ferromagnetic order. The magnetic long range order stays intact. This means that at low temperatures no magnetic phase transition will be caused by increasing pressure since the nickel concentration is above the percolation threshold. As long as we deny a considerable volume dependence of the nickel moment, this result is a consequence of our premise that the nickel atoms are characterized by local moments which do not depend on the electronic properties of the surrounding iron atoms. However, this assumption may not hold: *Ab initio* electronic structure calculations of $\mathrm{Fe}_3\mathrm{Ni}$ [4] show that iron and nickel moments diminish simultaneously at low volume.

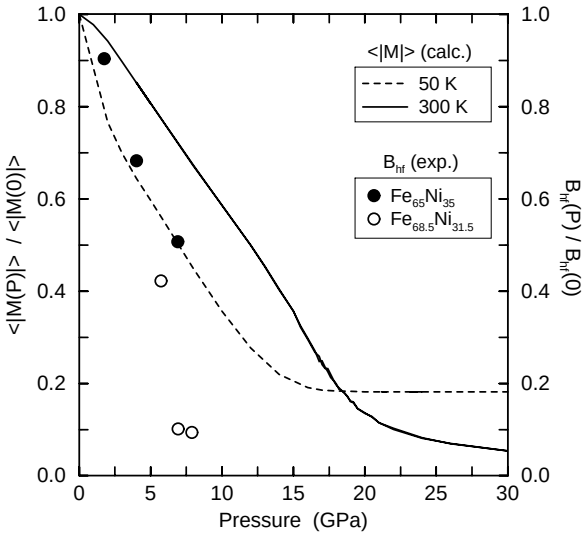

Fig. 15. Calculated pressure dependence of the magnetization for $Fe_{65}Ni_{35}$ (lines) and the average hyperfine field at $T = 4.2$ K (circles) as given by Mössbauer experiments (data taken from [47]).

6 Conclusion

Our simulations show that some of the most important thermodynamical properties of Invar alloys, as there is reduced thermal expansion, weakening of the elastic constants or broadening of the anomaly in the specific heat at T_C, can be accounted for by the HM-LM picture. This is remarkable since neither are Lennard-Jones potentials able to describe the elastic behavior of metals correctly nor are localized Ising spins believed to give an adequate representation of the magnetic properties of Invar alloys. Both were used because they are easy to compute and provide a tractable way to examine the thermodynamics of a system with HM-LM characteristics. The investigation of a homogeneous system consisting of atoms of only one type showed, that starting from a ferromagnetic HM ground state a first order HM-LM transition connected with a discontinuous contraction of the lattice constant might occur at low temperatures. Disfavoring the LM state by altering the energetics of our model shifts the magnetovolume effects to higher temperatures. But the first order transition disappears due to the influence of lattice vibrations which level out the energy barrier discouraging an intermixing of HM and LM bonds. In this case, the number of thermally excited LM sites increases gradually, leading to continuous magnetovolume effects.

The inclusion of chemical disorder as well as the use of antiferromagnetic exchange couplings between iron atoms for the description of Fe-Ni alloys play an important role for the qualitative accordance we achieved: Previous calculations with chemical disorder and a positive J_{FeFe} [49] also revealed smeared out magnetovolume effects. But around T_C considerable effects in α and B_S and a sharply peaked specific heat were encountered, resembling those obtained for the monatomic calculations (Figs. 5,6). So the smeared out minimum of the thermal expansion seems indeed to be caused by disorder, whereas the absence of considerable magnetovolume effects around T_C and the flattening of the anomaly in c_p are presumably due to the antiferromagnetic exchange coupling between iron atoms. Furthermore the variation of the number of antiferromagnetic Fe-Fe couplings at different compositions accounts for the change in the shape of the temperature dependence of α, B_S and c_p, which is close to the experimentally observed behavior. Although not all aspects of disordered systems can be discussed properly for small system sizes ($L \leq 12$), our simulations yield quantitatively reproducible results for the larger systems. Note also, that this is the first successful simulation of the smearing out of c_p, which is not an order of magnitude different from experimental results.

Future investigations should make use of distance dependent exchange constants, especially between iron atoms. As mentioned earlier, band structure calculations by Sabiryanov *et al.* [16] predict that the exchange coupling in fcc Fe depends sensitively on the distance between nearest neighbors which even includes a change of its sign from antiferromagnetic to ferromagnetic behavior. Recently, efforts have been made by Grossmann *et al.* [17] to explain magnetoelastic features of Invar materials by simulating a compressible Ising model. Their results show some analogy to our monatomic calculations. So a combined approach may yield further improvement, although one will face the problem of fixing even more parameters. We did not attempt this so far, since we wanted to single out the influence of lattice vibrations and competing exchange interactions first. Further improvements might be made by taking care of the strain induced by different equilibrium neighbor distances for iron and nickel atoms, which we neglected for the sake of simplicity. Since iron and nickel atoms are randomly placed on the lattice, this could alter the energy balance for a HM-LM flip in a similar way as the introduction of atom dependent exchange constants.

Finally we should compare our results to theoretical work based on continuous Ginzburg-Landau like spin models, as cited in the introduction. The advantage of such models is that here parameters can be well fitted to *ab initio* results for the magnetic binding surfaces and that the evolution of stable and metastable magnetic states with temperature can easily be calculated. The disadvantage, however, is that fluctuation effects appear in an exaggerated way at high temperatures which can only be handled very approximately by using temperature dependent cut-off parameters for the number of classical fluctuation modes. Also critical behavior cannot be described correctly within this type of fluctuation theory. The drawbacks of our present model (at low temperatures) have been discussed in the text; the advantage of our approach, however, is its simplicity. The consequences of the approximations we made (Ising magnetism, Lennard-Jones pair potentials) are well known, new effects can be studied by

gradually introducing new interactions or changing the interplay between existing ones by altering the parameters. This may help to understand the complex relationship of the many possible causes constituting the variety of Invar anomalies.

We wish to thank the Deutsche Forschungsgemeinschaft which has supported part of this work through the Sonderforschungsbereich 166. We also thank the HLRZ (KFA Jülich) since part of the work was done on their INTEL-Paragon parallel computer.

References

1. C.E. Guillaume, C.R. Acad. Sci. **125**, 235 (1897).
2. E.F. Wassermann, in *Ferromagnetic Materials*, Vol. 5, edited by K.H.J. Buschow, E.P. Wohlfarth, (Amsterdam: Elsevier, 1990), p. 237.
3. M. Shiga, in *Materials Science and Technology*, Vol. 3B, edited by R.W. Cahn, P. Haasen, E.J. Kramer (Weinheim: VCH, 1994), p. 159.
4. P. Entel, E. Hoffmann, P. Mohn, K. Schwarz, V.L. Moruzzi, Phys. Rev. B **47**, 8706 (1993).
5. E. Hoffmann, P. Entel, K. Schwarz, P. Mohn, J. Magn. Magn. Mater. **140-144**, 237 (1995).
6. M. Schröter, H. Ebert, H. Akai, P. Entel, E. Hoffmann, G.G. Reddy, Phys. Rev. B **52**, 188 (1995).
7. R.J. Weiss, Proc. Phys. Soc. (London) **82**, 281 (1963).
8. P. Entel, M. Schröter, Physica B **161**, 121 (1989).
9. D. Wagner, J. Phys. Cond. Matter **1**, 4635 (1989).
10. M. Schröter, P. Entel, S.G. Mishra, J. Magn. Magn. Mater. **87**, 163 (1990).
11. P. Mohn, K. Schwarz, D. Wagner, Phys. Rev. B **43**, 3318 (1991).
12. M. Uhl, J. Kübler, Phys. Rev. Lett. **77**, 334 (1996).
13. K. Takahashi, Prog. Theor. Phys. **79**, 997 (1988).
14. K. Takahashi, Z. Phys. B **71**, 205 (1988).
15. H.C. Herper, E. Hoffmann, P. Entel, Contribution submitted to ESOMAT '97.
16. R.F. Sabiryanov, S.K. Bose, O.N. Mryasov, Phys. Rev. B **51**, 8962 (1995).
17. G. Grossmann, D.G. Rancourt, Phys. Rev. B **54**, 12294 (1996).
18. D.G. Rancourt, M.-Z. Dang, Phys. Rev. B **54**, 12225 (1996).
19. Some work is in progress by performing *ab initio* molecular dynamics for Fe-Ni alloys: E. Hoffmann, P. Entel, J. Hafner, unpublished data.
20. M. Blume, Phys. Rev. **141**, 517 (1966).
21. H.W. Capel, Physica **32**, 966 (1966).
22. H.J. Gerber, K.D. Usadel, J. Magn. Magn. Mater. **73**, 327 (1988).
23. M.P. Allen, D.J. Tildesley, Computer Simulation of Liquids (Oxford: Clarendon, 1987).
24. B. Rellinghaus, J. Kästner, E.F. Wassermann, P. Mohn, Phys. Rev. B **51**, 2983 (1995).
25. G. Hausch, J. Phys. Soc. Jpn **37**, 819 (1974).
26. H.W.J. Blöte, E. Luijten, J.R. Heringa, J. Phys. A **28**, 6289 (1995).
27. D.M. Saul, M. Wortis, D. Stauffer, Phys. Rev. B **9**, 4964 (1974).
28. A.K. Jain, D.P. Landau, Phys. Rev. B **22**, 445 (1980).
29. A.I. Larkin, S.A. Pikin, Sov. Phys. JETP **29**, 891 (1969).
30. D.J. Bergman, B.I. Halperin, Phys. Rev. B **13**, 2145 (1976).
31. P. Entel, N. Grewe, J. Magn. Magn. Mater. **13**, 195 (1978).
32. P. Entel, N. Grewe, M. Sietz, K. Kowalski, Phys. Rev. Lett. **43**, 2002 (1979).
33. K. Binder, Z. Phys. B **43**, 119 (1981).
34. M. Shiga, H. Wada, H. Nakamura, K. Yoshimura, Y. Nakamura, J. Phys. F **17**, 1781 (1987).
35. M. Shiga, Physica B **149**, 293 (1988).
36. M.B. Taylor, B.L. Gyorffy, C.J. Walden, J. Phys. Cond. Matter **3**, 1575 (1991).
37. M.-Z. Dang, M. Dubé, D.G. Rancourt, J. Magn. Magn. Mater. **147**, 133 (1995).
38. A.J. Holden, V. Heine, J.H. Samson, J. Phys. F: Met. Phys. **14**, 1005 (1984).
39. E.F. Wassermann, P. Entel, J. Phys. IV France **5**, C8-287 (1995).
40. M. Shiga, K. Makita, K. Uematsu, Y. Muraoka, Y. Nakamura, J. Phys. Cond. Matter **2**, 1239 (1990).
41. P. Renaud, Thesis, University of Lausanne (1988).
42. B. Rellinghaus, J. van Lier, M. Röttker, J. Kästner, E.F. Wassermann, to be published.
43. W. Bendick, H.H. Ettwig, W. Pepperhoff, J. Phys. F **8**, 2525 (1978).
44. T.L. Polgreen, Phys. Rev. B **29**, 1468 (1984).
45. D.F. Styer, Phys. Rev. B **31**, 393 (1985).
46. A.B. Harris, J. Phys. C **7**, 1671 (1974).
47. M.M. Abd-Elmeguid, B. Schleede, H. Micklitz, J. Magn. Magn. Mater. **72**, 253 (1988).
48. M.M. Abd-Elmeguid, H. Micklitz, Physica B **161**, 17 (1989).
49. M.E. Gruner, Diplomarbeit, Gerhard-Mercator-Universität – GH – Duisburg (1995).